



How Does the Soil Chemical Composition Affect Its Cross-sections, Effective Atomic Number and Electron Density? Computer Simulation Analysis to Highlight the Radiation-soil Interaction Processes

Mario Augusto Camargo^{1,2}  · Karuane Schechtel Kodum²  · Luiz Fernando Pires³ 

Received: 22 February 2022 / Accepted: 23 June 2022 / Published online: 2 July 2022
© The Author(s) under exclusive licence to Sociedade Brasileira de Física 2022

Abstract

The study of radiation interaction parameters in complex materials (e.g., soils) has gained great importance in the last decades. However, few studies have directly addressed in detail how the radiation interaction is affected by the chemical and physical characteristics of soils, especially in tropical and subtropical climate regions like Brazil. The soil is an important material widely utilized in agriculture and engineering. Knowing this material radiation interaction properties is fundamental to understand its role in different areas of applied sciences such as radiation shielding, environmental monitoring, and geological characterization. This study presents a detailed analysis of how parameters like the atomic (σ_A), molecular (σ_M), and electronic (σ_E) cross-sections are affected by the texture and chemical composition of soils. The effective atomic number (Z_{eff}) and electron density (N_{el}) were also investigated. Photon energies in the energy range from 10 to 1330 keV were selected. The XCOM computer code was chosen to simulate the radiation interaction parameters. Five soils presenting different physical characteristics and oxide compositions were studied. The results show a strong dependence of the radiation interaction parameters on the elemental composition up to 100 keV. After this photon energy, factors such as fractional abundance, for example, become important to discriminate the soils. The parameters σ_A , σ_E , and Z_{eff} followed the same trend as that of the percentage of the oxides Fe_2O_3 and TiO_2 among soils, while σ_M and N_{el} matched the oxides SiO_2 and Al_2O_3 . Our results highlight that understanding how the chemical composition influences the radiation interaction in complex materials provides information that can be useful in areas such as radiation shielding and image analysis and processing, which are based on radiation interaction data.

Keywords XCOM · Mass attenuation coefficient · Tropical and subtropical soil · Radiation interaction

1 Introduction

Understanding the radiation interaction with the matter is fundamental to understand the processes of attenuation, absorption, and scattering of photons in complex materials such

as soil [1]. For example, in computed tomography studies, high-resolution images of soils are obtained after the interaction of photons (e.g., γ -rays) with this porous material [2–7]. Radiation attenuation data can be converted, after proper calibrations, into tomographic units (Hounsfield units) [8]. Several soil physical properties (e.g., moisture, bulk density, porosity) calculated based on tomography are sensitive to the image quality, which is closely related to the conversion of the attenuation data into tomographic units [9]. Thus, the understanding of how radiation interacts with complex materials such as soil can, for example, be useful for applied studies like the analyses of tomographic data [10–12].

In the process of radiation interaction with matter, photons can interact with the atom (or molecule), the atomic nucleus, and the orbital electrons. The cross section (σ) is the parameter that represents the probability that one of these interactions might occur [13]. Depending on the interaction

✉ Mario Augusto Camargo
mario.camargo@ifsc.edu.br

¹ Federal Institute of Education Science and Technology of Santa Catarina, Canoinhas Campus, Santa Catarina, Brazil

² Physics Graduate Program, Physics Department, State University of Ponta Grossa, Ponta Grossa, Brazil

³ Laboratory of Physics Applied to Soils and Environmental Sciences, Physics Department, State University of Ponta Grossa, Ponta Grossa, Brazil

considered, the abundance and chemical characteristics of the soil will allow the determination of the molecular (σ_M), atomic (σ_A), and electronic (σ_E) cross sections. Furthermore, as a heterogeneous medium, the incident photons are expected to interact differently with each fraction (clay, sand, silt) of the soil. Thus, it becomes impossible to define a single atomic number (Z) for the soil, which is achieved for pure elements. The effective atomic number (Z_{eff}) is the the elements found in these materials. Another parameter that is closely related to Z_{eff} and provides information about how radiation interacts with the soil is the electron density (N_{el}) [14], which represents the number of electrons per unit mass. N_{el} is related to the probability of finding any one of the electrons in a specific location around an atom (or molecule) [15]. It is important to highlight that all these parameters are strongly dependent on the photon energy (E) [16].

Torikoshi et al. [10] used a dual-energy computed tomography system to obtain images from N_{el} and Z_{eff} data following their own methodology. The authors obtained high-quality images, which clearly depicted the structures of the samples. Although Torikoshi et al. [10] examined biological samples, the methodology proposed by them can be applied to other materials such as soil, and in this sense, the knowledge of how the radiation interaction parameters are influenced by the chemical composition or other factors can result in the development of high-quality images.

Analyses based on radiation interaction processes (tomography, radiation shielding, γ -ray attenuation, etc.) provide data that are directly related to the mass attenuation coefficient (μ) of the materials that found in the soil [12]. Tropical and subtropical soils are complex materials having their chemical composition consisting mostly of oxides such as SiO_2 , Al_2O_3 , Fe_2O_3 , and TiO_2 [17, 18]. However, the number of studies showing possible correlations between the radiation interaction parameters, the chemical composition, and the granulometric fractions (texture) of tropical and subtropical soils is still low. In tropical and subtropical regions characterized by hot and humid climates, weathering is a process that occurs more severely and intensely. The soil formation processes are also more active and often continuous, mainly due to differences in climate and biological processes [19]. Thus, the weathering action reflects on the constituents and texture of the soil. Studying the relationships between the soil constituents, weathering, and the radiation interaction parameters might also be useful to understand how these parameters can be influenced by the soil formation [20]. As recently demonstrated by Camargo et al. [18], μ is influenced by the chemical composition of the soil, which is closely related to its texture. Thus, changes in soil texture will affect μ with direct impacts on the measurement of physical properties based on radiation interaction [21–23].

This study aimed to analyze the effect of the chemical composition and texture of tropical and subtropical soils,

exposed to different levels of weathering, on the parameters σ_M , σ_A , σ_E , Z_{eff} , and N_{el} . The photon energy range investigated varied from 10 to 1330 keV, due to the frequent use of these energies in studies on radiation interaction with soils. The parameters analyzed were derived from the μ values obtained via the XCOM computer code [24]. The option to investigate using this program was due to its availability, speed, ease of use, and the number of scientific studies that use it [5, 12, 25, 26], even though there are other tools that can also be used in this kind of study, e.g., GEANT4, FLUKA, and MCNP [27]. The novelties of this research include (1) detailed analysis of the parameters (e.g., molecular weight, number of formula units, fractional abundance, etc.) that influence the cross sections (σ_M , σ_A , and σ_E) as a function of soil composition, (2) investigation of the relation between weathering and soil texture on radiation interaction, and (3) the influence of major oxides in tropical and subtropical soils in Z_{eff} and N_{el} .

2 Materials and methods

Five soils with distinct contents of the four major oxides usually found in tropical and subtropical soils were selected (SiO_2 , Al_2O_3 , Fe_2O_3 , and TiO_2) for this study. The soils identified as 1 and 2 in this report are from Piracicaba—São Paulo State (22° 4' S; 47° 38' W; 580 m above sea level), 3 is from Pato Bragado—Paraná State (24° 37' S; 54° 13' W; 282 m above sea level), 4 is from Ponta Grossa—Paraná State (25° 09' S; 50° 16' W; 975 m above sea level), and 5 is from Paranavaí—Paraná State (23° 04' S; 52° 27' W; 446 m above sea level) (Fig. 1).

Based on the elemental analysis (oxide composition) of the soils, the mass attenuation coefficients were calculated. The oxide compositions (major oxides) and granulometric fractions (Table 1) of the first four soils (soils 1 to 4) were obtained from the data presented in the study by Medhat et al. [28]. The soils were chosen based mainly on the differences found in sand, silt, and clay contents. For the granulometric analysis, the pipette method [29] was selected, which is based on the difference in the speed of deposition of soil particles in a $NaOH$ dispersant solution. The sand fraction was firstly separated by sieving and the other fractions (silt and clay) by decantation. The sedimentation time for the silt particle was estimated by Stokes' law, and the remaining volume of the suspension was pipetted to determine the clay fraction.

The elemental analysis was carried out using an energy dispersive X-ray fluorescence spectrometer (Shimadzu, model EDX-720). The equipment has a rhodium (Rh) tube with the voltage unit ranging from 5 to 50 kV and filament operating currents from 1 to 1000 μA . The detector is a $Si(Li)$



Fig. 1 Map of Brazil. The area highlighted in red on the map has been enlarged and shows locations of the four cities where soil samples were collected. Satellite image courtesy © Google, Data SIO, NOAA, U.S. Navy, NGA, GEBCO

semiconductor, which works with liquid nitrogen maintained at -196°C . For the measurements, the soil samples were macerated in pistils, placed in a sample holder provided by the equipment manufacturer, and sealed with Mylar ($6 - \mu\text{m}$ thickness). The time taken to obtain the spectrum was 100 s, in the sodium to scandium ($Na - Sc$) (15kV) and titanium to uranium ($Ti - U$) (50kV) energy bands. All measurements were carried out under 30Pa pressure in semi-quantitative mode [30]. In this study, we considered soils composed mostly of the SiO_2 , Al_2O_3 , Fe_2O_3 , and TiO_2 oxides, since these were the most abundant oxides found in the five soil samples.

From the percentage of oxides, the values of μ were calculated through the XCOM (Version 1.5) computational code [24], which is based on the mixture rule. This software provides data of the total and partial (coherent and incoherent scatterings, photoelectric effect, and pair production) μ for elements, compounds, and mixtures having atomic number ranging from 1 to 100. The photon energy range covered by the XCOM computational code varies from 1keV to 100GeV. The $(\text{cm}^2\text{g}^{-1})$, for compounds and mixtures, can be found from the contribution of the elements constituting the material and their respective weight fractions [31]:

$$\mu = \sum (\mu)_i W_i \tag{1}$$

where $(\mu)_i$ represents the mass attenuation coefficient of the i th element and W_i represents its weight fraction, which is obtained from the following relationship:

$$W_i = \frac{n_i A_i}{\sum n_j A_j} \tag{2}$$

where A_i is the atomic mass of the i th element (gmol^{-1}), n_i is the number of formula units, and $\sum n_j A_j$ is the sum of the atomic mass and formula unit number of the elements in the material.

Since μ results from the contributions of partial effects such as coherent and incoherent scatterings, photoelectric effect, and pair production, its values are strongly influenced by the photon energy and the atomic number (Z) of the elements found in the soil. Regarding low-energy photons (30keV), greater contribution of the photoelectric effect (dependence directly proportional to Z^{4-5}) to the radiation attenuation is observed, while at intermediate energies (150keV to 3MeV), the incoherent scattering is the most important effect (linear dependence with Z) [13, 32].

Table 1 Percentage of the major oxides and granulometric fractions for the different soils studied

Soil	Oxides (%)				Granulometry (%)		
	SiO_2	Al_2O_3	Fe_2O_3	TiO_2	Sand	Silt	Clay
1	65	30	3	2	66	6	28
2	47	33	17	3	26	26	48
3	33	35	28	4	18	20	62
4	32	52	14	2	17	22	61
5	77	19	3	1	91	1	8

As described before, each of the partial interaction processes has a direct dependence on the atomic number of the absorber [33]. However, since soils represent complex materials, it is not possible to define a single atomic number for each interaction process, so that Z_{eff} is defined. The effective atomic number is a parameter that directly depends on the contribution of the partial interaction processes, causing its dependence on the Z values of the elements that constitute the material. The values of Z_{eff} are strictly linked to N_{el} [16], another parameter of interest when the radiation interaction with complex materials is studied.

When photons interact with the matter, this interaction might occur with individual atoms, molecules, and orbital electrons, so it is possible to calculate cross sections (molecular, atomic, and electronic) for each of these types of interaction. The photon interaction at the molecular level is given by [31]:

$$\sigma_m(\text{b molecule}^{-1}) = \mu \left(\frac{M}{N_A} \right) \quad (3)$$

where N_A is Avogadro's number and M is the sum of the molecular weights of the mixture, which is directly proportional to the sum of the number of formula units and their respective atomic masses (A_i):

$$M = \sum n_i A_i \quad (4)$$

The interaction with the atomic nucleus can be written as a function of the molecular cross-section and the sum of formula units of the mixture ($\sum n_i$):

$$\sigma_a(\text{b atom}^{-1}) = \sigma_m \left(\frac{1}{\sum n_i} \right) \quad (5)$$

Finally, the interaction with the electron orbital, that is, at the electronic level, can be written as a function of the fractional abundance (f_i), μ , A , and Z of the elements found in the complex media:

$$\sigma_e(\text{b electron}^{-1}) = \frac{1}{N_A} \left(\sum \frac{f_i A_i}{Z_i} (\mu)_i \right) \quad (6)$$

with f_i calculated as follows:

$$f_i = \frac{n_i}{\sum n_j} \quad (7)$$

where $\sum n_j$ is the total number of atoms in the molecular formula.

Following the calculation of the cross sections, it is possible to determine the value of Z_{eff} [34]:

$$Z_{eff} = \frac{\sigma_a}{\sigma_e} \quad (8)$$

The electron density N_{el} (electrons g^{-1}) of a material, the last parameter analyzed in our study, can be written as a function of μ and σ_e , as well as Z_{eff} and M :

$$N_{el} = \frac{\mu}{\sigma_e} = \left(\frac{Z_{eff}}{M} \right) N_A \sum n_i \quad (9)$$

In this study, the photon energy range from 10 to 1330keV was selected to analyze the radiation interaction parameters (σ_M , σ_A , σ_E , Z_{eff} and N_{el}). Other four specific photon energies were chosen referring to the ^{241}Am (59.54keV), ^{133}Ba (356keV), ^{137}Cs (661.6keV), and ^{60}Co (1330keV) radioactive sources. The selection of these additional energies, as well as the photon energy range, is due to the frequent use of these energies in studies on radiation interaction with soils [35, 36]. Moreover, the same photon energies were investigated in a previous study performed by Camargo et al. [18], for which this work is a sequence. However, it is important to highlight that our study does not present any experimental measurements of the radiation interaction parameters, since our main objective was to use simulation to verify the effect of the chemical composition of soils, weathering, and granulometric fractions on interaction parameters across different photon energy ranges.

Aiming to verify the existence of possible correlations between the radiation interaction parameters and other soil characteristics (chemical composition (major oxides), weathering index ($K_i = (\text{SiO}_2/\text{Al}_2\text{O}_3) \times 1.7$) [37], and granulometric fraction), a multiple linear regression analysis was performed. The analyses were conducted at 59.54, 356, 661.6, and 1330keV photon energies to verify the influence of low, intermediate, and high photon energies in the radiation interaction parameters. All statistical analyses were performed using the PAST (PAleontological STatistics) software [38].

3 Results

The μ variation as a function of E in the five different soils studied is presented (Fig. 2). The photon energy range (1 to 10^5keV) selected in Fig. 2a emphasizes the regions where the radiation interaction partial effects (coherent and incoherent scatterings, photoelectric effect, and pair production) with soils were predominant. The hatched area delimits the energy range (10 to 1330keV) commonly employed in measurements of soil physical properties through radiation methods, by encompassing characteristic energy ranges of stable elements for analyses involving radiation [1, 28, 30]. An analysis of the μ variation in this energy range is shown in Fig. 2b.

A decrease in the μ value was observed when the photon energy increased in all soils analyzed as expected (Fig. 2)

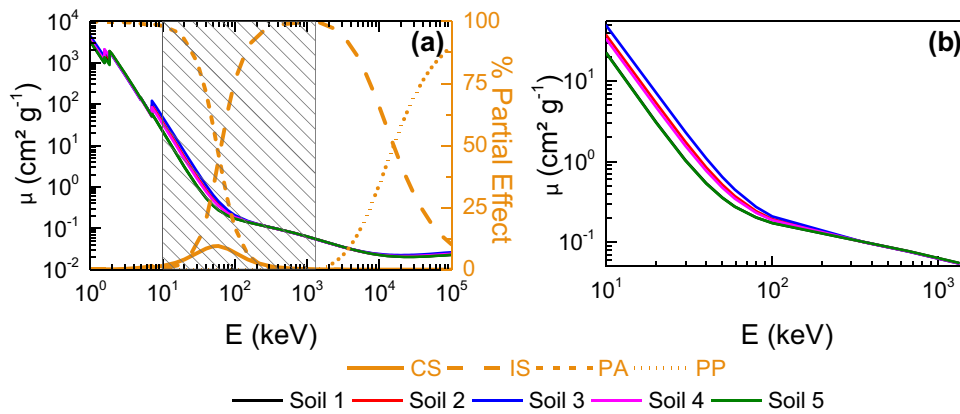


Fig. 2 Mass attenuation coefficient (μ) as a function of photon energy (E) for the five soils analyzed. **a** The energy range extends from 1 to 10^5 keV, showing the different percentages of the partial effects of the interaction of radiation with matter (coherent (CS) and incoherent (IS) scattering, photoelectric effect (PA), and pair production (PP)).

The hatched area corresponds to the main energy range used in soil studies. The percentages of the partial effects were calculated based on the contributions of each partial effect relative to the total μ for soil 4. **b** Variation of μ in the energy range from 10 to 1330 keV

[18, 30], showing that at lower E , there is a separation of the characteristic spectra of each soil having contrasting chemical compositions (Fig. 2b). Soil 3 presented the highest μ when compared to the other soils (soil $2 > 4 > 1 > 5$) for $E < 100$ keV. Nonetheless, for $E > 100$ keV, the curves converge presenting small differences between them. The correlation analysis (Online Resource 1—Table 1) demonstrated that for photons with $E < 100$ keV, specifically for those of 59.54 keV, positive linear relationships occurred between the pairs $Fe_2O_3 \times \mu$ ($r = 0.999$) and $TiO_2 \times \mu$ ($r = 0.927$). The same behavior was observed for the pairs of clay $\times \mu$ ($r = 0.833$) and silt $\times \mu$ ($r = 0.769$).

The last results indicate that the tropical and subtropical soils with the highest amounts of clay and silt were also those with the highest Fe_2O_3 and TiO_2 contents. This fact was confirmed by the correlation analysis between these two oxides and clay ($r = 0.845$ – Fe_2O_3 ; $r = 0.768$ – TiO_2) and silt ($r = 0.779$ – Fe_2O_3 ; $r = 0.706$ – TiO_2) contents. Thus, a possible explanation for the results observed in Fig. 2, that is, the separation between the curves, is the differences found in the chemical composition and granulometric fractions of the contrasting soils studied [18, 28, 39]. This might result in the distinction of spectra and may also be caused by information intrinsic to soils such as its mineralogy and organic content. However, it seems relevant to mention that the correlation analysis presented, only intended to give an idea of the possible effects of the soil chemical composition and its granulometry on the radiation interaction parameters. More detailed analysis on this subject should include a larger number of soils with contrasting characteristics.

The σ_M (Fig. 3a), σ_A (Fig. 3b), and σ_E (Fig. 3c) variations as a function of E for the five soils studied are presented

below (Fig. 3). The cross-section (molecular, atomic, and electronic) values decreased increasing E , as evidenced by other results already reported in the scientific literature [28]. The curves presented small differences between each other for $E < 100$ keV, but at higher photon energies, soil 5 is the one exhibiting the highest σ_M (soil $1 > 4 > 2 > 3$) (Fig. 3a).

Similar behavior was observed for the σ_A and σ_E parameters, in which the greatest differences among soils occurred for $E < 100$ keV (Figs. 3b, c). The following sequence in the σ_A or σ_E values ($E < 100$ keV) was found: soil $3 > 2 > 4 > 1 > 5$ (the last two overlapping). For $E > 100$ keV, σ_A and σ_E converged practically do not present differences among soils. Contrary to σ_A and σ_E , σ_M presented the greatest differences among soils for $E > 100$ keV. An inversion was also found in the soils order for σ_M (soil $3 < 2 < 4 < 1 < 5$) relative to σ_A and σ_E .

To explain the σ_M results, its values were analyzed as a function of M for the five soils at the 20, 30, 40, 59.54, and 661.6 keV photon energies (Fig. 4a). We observed that the increase in the photon energy decreased the dependence between σ_M and M . This result shows that the sum of the molecular weights of the soil compounds explains the inversions in the sequence of σ_M curves when compared to σ_A and σ_E (with the highest value now having the lowest value and vice versa) observed in the curves among soils, regardless of their μ values (Fig. 2a). The parameter σ_A (Fig. 4b) was evaluated as a function of $\sum n_i$ Eq. (5) for the same photon energies as presented in Fig. 4a. An inverse relation was observed between σ_A and $\sum n_i$, with a lower dependence of these two parameters at higher energies.

The last analysis might explain the inversion observed in the sequence of curves (now changing from 3 to 5) between the σ_A curves for the contrasting soils studied. The linear

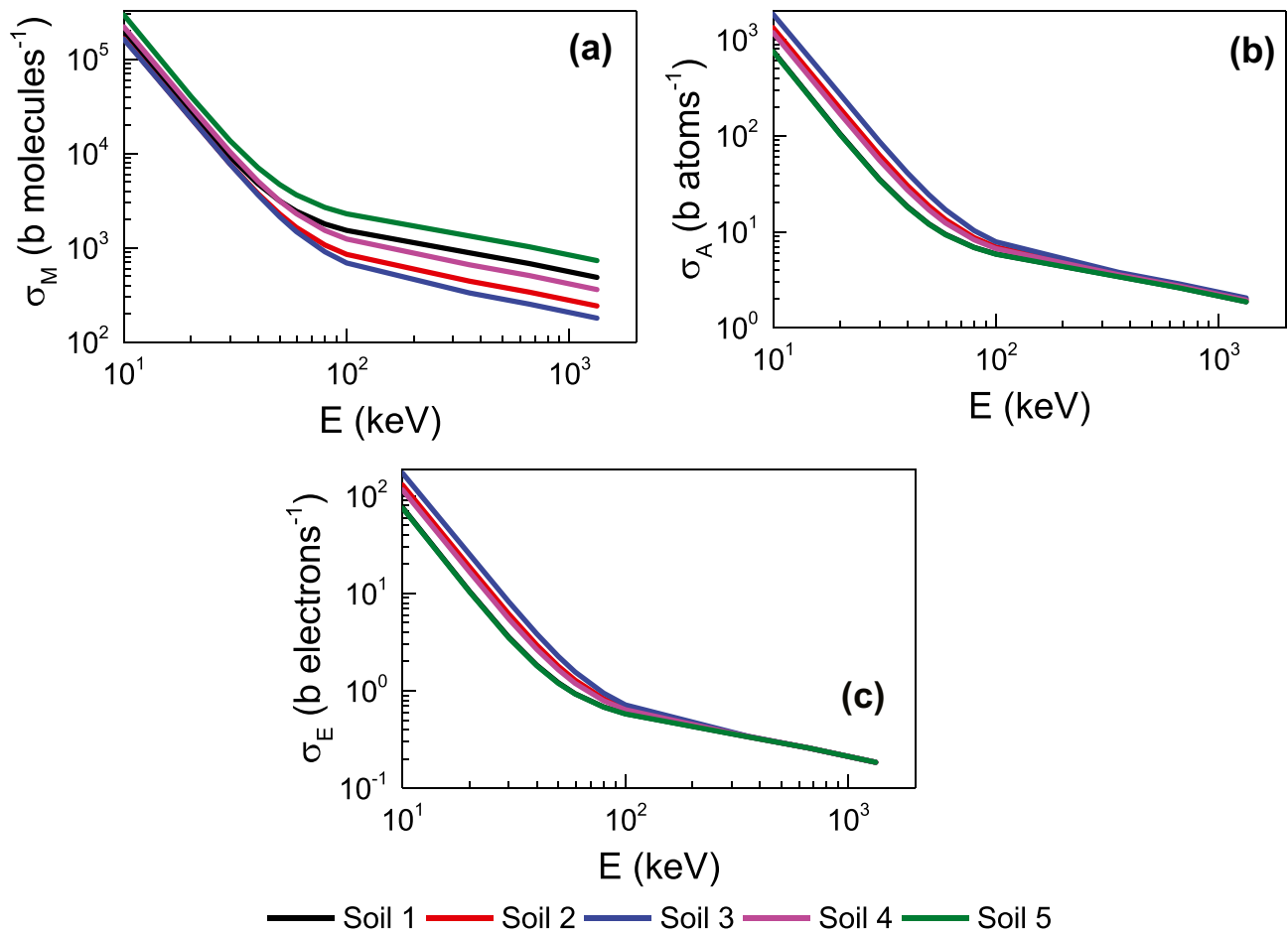


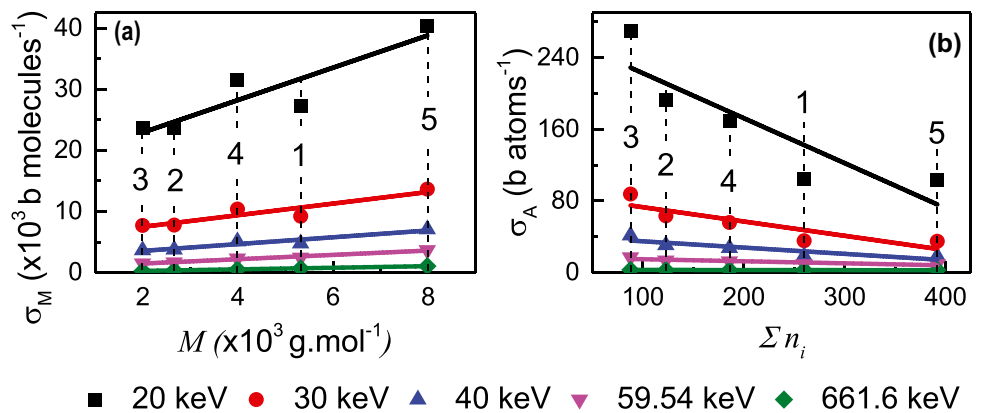
Fig. 3 **a** Molecular cross-section (σ_M), **b** atomic cross section (σ_A), and **c** electronic cross section (σ_E) as a function of photon energy (E) for the five soils studied

correlation analyses (Online Resource 1—Table 1) at the 59.54keV photon energy confirms the results obtained; a direct relationship between σ_M and M ($r = 0.989$) and an inverse relationship between σ_A and $\sum n_i$ ($r = -0.989$) were noticed. For the other photon energies (356, 661.6, and

1330keV), the behavior observed between these parameters remained similar.

The results of the linear correlation analysis (Online Resource 1—Table 1) at the 59.54keV energy showed that σ_M was inversely related to clay ($r = -0.859$), silt

Fig. 4 **a** Molecular cross-section (σ_M) as a function of the sum of the molecular weights of the mixture (M) for the soils at five photon energies. **b** Atomic cross-section (σ_A) as a function of the sum of formula units of the mixture ($\sum n_i$). The vertical dashed lines indicate M and $\sum n_i$ of each soil (1–5) studied. The colored straight lines represent linear fits for each specific photon energy



($r = -0.846$), Fe_2O_3 ($r = -0.826$), and TiO_2 ($r = -0.932$) contents. Thus, increases in the amounts of these oxides and silt and clay granulometric fractions reduced σ_M at lower energies. Similar behavior was observed at the higher energies (356, 661.6, and 1330keV) investigated (Online Resource 1—Tables 2, 3, and 4). Inverse linear relationships were also found between σ_M and μ ($r = -0.830$). For the parameters σ_A and σ_E , similar to the results observed for μ , positive linear relationships were found between the pairs $\sigma_A \times \text{clay}$ ($r = 0.828$), $\sigma_E \times \text{clay}$ ($r = 0.837$), $\sigma_A \times \text{silt}$ ($r = 0.754$), $\sigma_E \times \text{silt}$ ($r = 0.773$), $\sigma_A \times Fe_2O_3$ ($r = 0.999$), $\sigma_E \times Fe_2O_3$ ($r = 1.000$), $\sigma_A \times TiO_2$ ($r = 0.928$), and $\sigma_E \times TiO_2$ ($r = 0.926$), at the 59.54keV photon energy.

The same type of relationship was observed at higher photon energies (Online Resource 1—Tables 2, 3, and 4), indicating that when E increases, the clay, silt, Fe_2O_3 , and TiO_2 contents have similar influence in the σ_A and σ_E parameters as that at lower E . The mass attenuation coefficient was also strongly related to σ_A ($r = 1.000$) and σ_E ($r = 1.000$) at the lowest energy (59.54keV), highlighting the close relation between these parameters (Figs. 2 and 3). An inverse relationship was also observed between SiO_2 and the σ_A ($r = -0.827$) and σ_E ($r = -0.836$) parameters in 59.54keV. A similar result was found at higher E (Online Resource 1—Tables 2, 3, and 4). These results demonstrate the great influence of the granulometric fractions, and the most common oxides found in tropical and subtropical soils in the radiation interaction parameters studied.

The electron density and effective atomic number as a function of E for the soils investigated are shown below (Fig. 5). In both cases, each soil presented a characteristic curve with similar behavior among them. We also noticed that three regions of E can be highlighted in our results. For $E < 30keV$, N_{el} (Fig. 5a), and Z_{eff} (Fig. 5b) had their lower values characterized by slight variations. However, for E between 30keV and 356keV (^{133}Ba), N_{el} and Z_{eff} presented an increasing trend in all soils; and finally, at higher E , N_{el} and Z_{eff} reached their highest values becoming approximately constant [28].

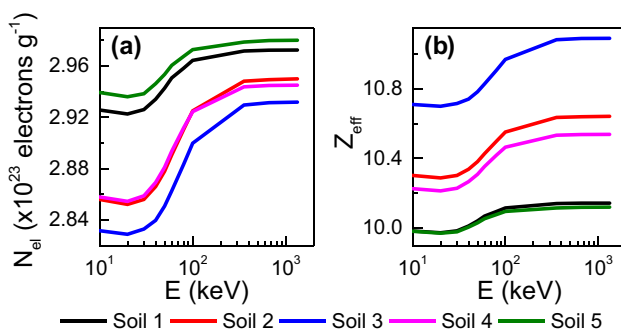


Fig. 5 a Electron density (N_{el}). b Effective atomic number (Z_{eff}) as a function of photon energy (E) for the soils studied

The electron density as a function of the sum of the concentrations of iron and titanium oxides (Fig. 6a) showed an inverse relationship mainly at lower E . The opposite was noticed when N_{el} was plotted as function of the sum of the concentrations of silicon and aluminum oxides (Fig. 6b). The effective atomic number, inversely to N_{el} , presented a direct relationship with the sum of the iron and titanium oxide concentrations as expected, with greater dependence on higher E (Fig. 6c). However, when Z_{eff} was plotted against the sum of the concentrations of silicon and aluminum oxides (Fig. 6d), the opposite was observed.

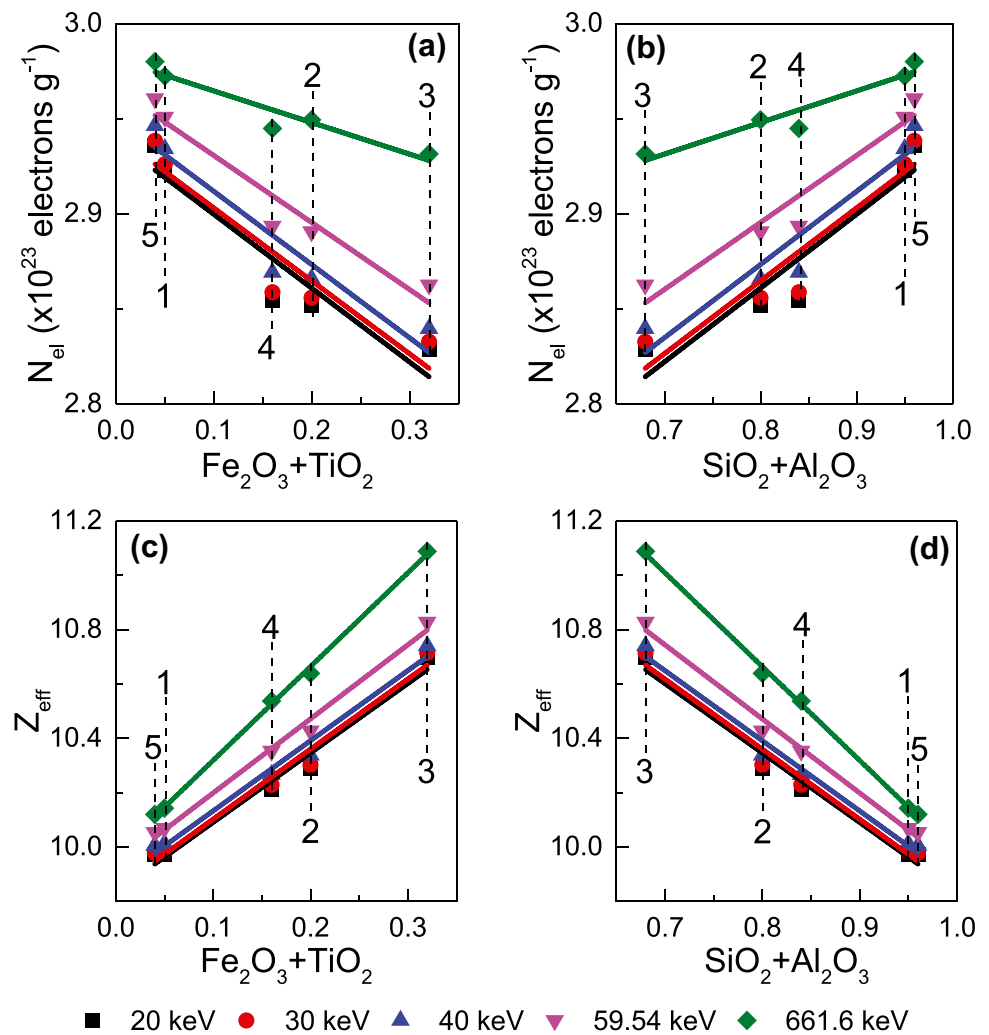
At the 59.54keV photon energy, the linear correlation analyses (Online Resource 1—Table 1) showed that N_{el} is inversely related to clay ($r = -0.938$), silt ($r = -0.896$), and $Fe_2O_3 + TiO_2$ ($r = -0.968$) amounts, although a direct relationship was observed between N_{el} and sand content ($r = 0.946$) and $SiO_2 + Al_2O_3$ ($r = 0.968$). The same behavior was found for the other E investigated (Online Resource 1—Tables 2, 3, and 4). Thus, we noticed that soils with higher clay, silt, and $Fe_2O_3 + TiO_2$ amounts tend to have lower N_{el} , while higher sand and $SiO_2 + Al_2O_3$ contents increase N_{el} (Fig. 5a). Also, Z_{eff} showed an opposite behavior to N_{el} in terms of the linear correlation coefficients (Online Resource 1—Tables 2, 3, and 4) as expected (Fig. 5b). The correlations between the pairs $N_{el} \times Fe_2O_3 + TiO_2$, $N_{el} \times SiO_2 + Al_2O_3$, $Z_{eff} \times Fe_2O_3 + TiO_2$, and $Z_{eff} \times SiO_2 + Al_2O_3$ confirmed the data presented in Fig. 6a–d.

Finally, the measured index (K_i) of soil weathering [37] presented an inverse relationship with the pairs $K_i \times \text{clay}$ and $K_i \times \text{silt}$, indicating that higher concentrations of these granulometric fractions implied a higher degree of weathering. However, it is important to emphasize that this type of analysis only serves to indicate how weathering could explain the results between soils, but for a more complete analysis, we suggest analyzing a larger set of soils under different weathering stages.

4 Discussion

The radiation interaction parameters investigated in this study presented noticeable distinct behavior among soils as a function of the photon energies studied. The different soil granulometric and chemical (oxides) compositions greatly influenced the parameters μ , σ_A , and σ_E at lower E . Regarding the σ_M parameter, the regions of intermediate and higher E were the most important for discriminating the different soil types studied. The parameters N_{el} and Z_{eff} showed differences among soils in the whole range of E analyzed, demonstrating that these two parameters are clearly sensitive to the chemical and granulometric composition of the soils [1, 40]. The influence of the soil particle size (granulometry) as well as its chemical composition significantly affect the radiation

Fig. 6 Electron density (N_{el}) as a function of the sum of the concentrations of **a** iron and titanium oxides and **b** silicon and aluminum oxides for the soils studied at specific photon energies. Effective atomic number (Z_{eff}) as a function of the sum of the concentrations of **c** iron and titanium oxides and **d** silicon and aluminum oxides. The vertical dashed lines indicate the values of the summed concentrations of the oxides for each of the soils (1–5) analyzed. The colored straight lines represent linear fits for each specific photon energy



interaction parameters studied, as proven by the linear correlation analyses carried out (Online Resource 1—Tables 1, 2, 3, and 4). The predominance of the different partial effects of radiation interaction (coherent and incoherent scattering, photoelectric effect, and pair production) explains the differences observed in the different E range investigated [1, 13, 16, 18].

When analyzing Fig. 2a, we verified a reversal trend in the contribution of the dominant partial effect at $\sim 100\text{keV}$, that is a transition from the predominance of the photoelectric effect to incoherent scattering. Since the dependence of the photoelectric effect is directly proportional to Z^{4-5} at lower E , we might conclude that the separation among the soil μ curves is mainly related to the differences found in the $\text{Fe}_2\text{O}_3 + \text{TiO}_2$ contents (Fig. 2b) [18, 34]. Soils 3 and 5 exhibited the highest and the lowest μ , respectively, as they are the soils with the highest and lowest $\text{Fe}_2\text{O}_3 + \text{TiO}_2$ amounts. However, in the region where the incoherent scattering (linear dependence with Z) was predominant, an overlap among the soil μ curves occurred demonstrating the

chemical composition irrelevance in this region to discriminate soils [18, 39].

Due to the influence of partial effects on μ [18] and the dependence of σ_M on M Eq. (3), an overlap of the curves up to the $\sim 100\text{keV}$ energy was observed (Fig. 3a), and their separation from this E onwards. The overlap observed for low E (photoelectric effect domain) is mainly associated with the relationship between the values of μ and M (Fig. 4a) due to the compensation of higher values of μ and lower values of M in this energy range, while the separation among curves above $\sim 100\text{keV}$ is related to the incoherent scattering and the values of M among soils (soil 5: the highest; soil 3: the lowest). The σ_M and M values had significant correlations with each other (Online Resource 1—Tables 1, 2, 3, and 4) so that the dependence between these two parameters is most sensitive at the lowest photon energies ($< 40\text{keV}$). However, an analysis of the increase in E demonstrated no variation in the slope of the σ_M and M straight lines, which might explain the separation between the curves among soils (Fig. 4a).

Among the factors that influence σ_A , one that has great relevance is the sum of formula units of the mixture ($\sum n_i$) [1, 16, 41], so that when the ratio of $\frac{M}{\sum n_i}$ is calculated, curves of variation of σ_A with E (Fig. 3b) that follow the order of the contents of $Fe_2O_3 + TiO_2$ were obtained, for each of the soils studied ($5 < 1 < 4 < 2 < 3$). Similar behavior was also observed for μ (Fig. 2b) and σ_E (Fig. 3c) due to the existing dependence between these parameters (Eqs. 5 and 6) [37]. The fractional abundance of the elements (f_i) is the factor with the greatest influence on σ_E (distinction between the curves) among the soils studied, in $E < 100keV$. We noticed that the soils possessing the highest f_i of $Fe_2O_3 + TiO_2$ ($5 < 1 < 4 < 2 < 3$) were those with the greatest σ_E . The convergence among the curves in $E > 100keV$ is mainly associated with the incoherent scattering and its probability of occurrence [42].

Considering that the Fe contribution in σ_E decreases from $\sim 100keV$ onwards, and the dependence of Z_{eff} with σ_E and σ_A Eq. (8), an increase in Z_{eff} occurs from this energy onwards (Fig. 5b). At lower photon energies ($< 100keV$), both soil μ and their constituent elements depend on Z^{4-5} , reducing Z_{eff} [30]. At higher photon energies ($> 100keV$), a reduction in the dependence of μ on the chemical composition of the soils tends to occur, so that the differences among the curves are mainly related to the $\frac{M}{\sum n_i}$ factor.

For N_{el} , its inverse dependence on σ_E and direct dependence on μ Eq. (9) explains the inversion of the sequence of curves observed among the curves (Fig. 5a). At lower photon energies ($< 100keV$), the soils with higher Fe amounts, and consequently higher μ , were those with higher σ_E , lowering N_{el} . At higher photon energies ($> 100keV$), σ_E had the greatest influence on N_{el} when all the soils were compared [28]. Considering the dependence of Z_{eff} and N_{el} on the soil chemical composition [1], the correlation between these parameters with the Fe_2O_3 and TiO_2 contents (Online Resource 1—Tables 1, 2, 3, and 4) demonstrated that the soils with higher values of this sum presented the highest values of Z_{eff} and consequently the lowest values of N_{el} (Fig. 6a, c). Meanwhile, when relating the sum of the SiO_2 and Al_2O_3 oxides (Fig. 6b, d), we noticed lower Z_{eff} values and higher N_{el} values. This result highlights the importance of the major soil oxides on radiation interaction parameters in tropical and subtropical soils.

Based on the results presented, we demonstrated that the granulometry and chemical composition of the soils had important influence in radiation interaction parameters. It seems relevant to emphasize that there are still few studies addressing a detailed analysis of radiation interaction parameters and characteristics associated with the soil formation, especially in soils from tropical and subtropical climates. Thus, our study reported a detailed investigation of the influence of factors that are intrinsically linked

to soil formation in the radiation interaction parameters. Additionally, we verified the photon energy ranges that are more sensitive to the differences observed in the soil characteristics studied. Correlation analyses were performed to verify how the soil characteristics influence radiation interaction parameters, so this study presented a detailed analysis of the relationship among different soil properties. However, we noticed that the results obtained in our study still need to be extended to larger amounts of soils with different physical and chemical characteristics. This suggestion aims to obtain more representative results of the influence of parameters related to soil formation and weathering in radiation interaction parameters, which unfortunately was not possible to carry out in our study.

5 Conclusion

Our research analyzed the effect of the chemical composition and granulometric fractions of tropical and subtropical soils with different levels of weathering in the σ_M , σ_A , σ_E , Z_{eff} , and N_{el} parameters in the photon energy range between 10 and 1330keV. The XCOM computational code was used in the analyses. We observed that at $E < 100keV$, the parameters μ , σ_A , and σ_E are sensitive to the chemical composition of the soils studied, mainly to their $Fe_2O_3 + TiO_2$ contents. The clay and silt fractions showed a strong correlation with the σ_A , σ_E , and Z_{eff} parameters at the 59.54, 356, 661.6, and 1330keV specific photon energies, while σ_M and N_{el} presented an inverse trend in the correlations. Direct correlations were also observed between the clay and silt fractions when compared to the $Fe_2O_3 + TiO_2$ content, as well as inverse correlations between the clay and silt fractions against the K_f index (related to weathering). A detailed analysis of the partial effects (coherent and incoherent scatterings, photoelectric effect, and pair production) and of a couple of variables (sum of the molecular weights of the mixture, fractional abundance, and sum of formula units of the mixture) sensitive to radiation interaction was carried out. The results showed that the soil granulometric fractions and the most common oxide contents found in tropical and subtropical soils have a great influence on radiation interaction parameters.

Supplementary Information The online version contains supplementary material available at <https://doi.org/10.1007/s13538-022-01159-8>.

Acknowledgements LFP would like to acknowledge the financial support provided by the Brazilian National Council for Scientific and Technological Development (CNPq) through Grant 304925/2019-5 (Productivity in Research). KSK would like to acknowledge the master grant provided by the Coordination for the Improvement of Higher Education Personnel (Capes).

Authors' contributions M.A. Camargo: Formal analysis, data curation, methodology, and writing—original draft. K.S. Kodum: Formal analysis, data curation, methodology, and writing—original draft. L.F. Pires: Conceptualization, data curation, and writing—original draft. The authors read and approved the final manuscript.

Declarations

Competing Interests The authors declare that they have no competing interests.

References

- N. Kucuk, Z. Tumsavas, M. Cakir, Determining photon energy absorption parameters for different soil samples. *J. Radiat. Res.* **54**, 578 (2013)
- F. A. M. Cássaro, A. N. Posadas Durand, D. Gimenez, C. M. Pedro Vaz, Pore-size distributions of soils derived using a geometrical approach and multiple resolution MicroCT images. *Soil Sci. Soc. Am. J.* **81**, 468 (2017)
- J.A.R. Borges, L.F. Pires, F.A.M. Cássaro, W.L. Roque, R.J. Heck, J.A. Rosa, F.G. Wolf, X-ray microtomography analysis of representative elementary volume (REV) of soil morphological and geometrical properties. *Soil Tillage Res.* **182**, 112 (2018)
- J.A.R. Borges, L.F. Pires, F.A.M. Cássaro, A.C. Auler, J.A. Rosa, R.J. Heck, W.L. Roque, X-ray computed tomography for assessing the effect of tillage systems on topsoil morphological attributes. *Soil Tillage Res.* **189**, 25 (2019)
- T.R. Ferreira, J.A.R. Borges, L.F. Pires, Representative elementary area for soil bulk density measurements of samples collected in volumetric rings by CT image analyses. *Soil Tillage Res.* **152**, 74 (2015)
- J.A.T. Oliveira, F.A.M. Cássaro, L.F. Pires, Estimating soil porosity and pore size distribution changes due to wetting-drying cycles by morphometric image analysis. *Soil Tillage Res.* **205**, 104814 (2021)
- J.A.T. Oliveira, F.A.M. Cássaro, L.F. Pires, Quantification of the pore size distribution of a Rhodic Hapludox under different management systems with X-ray microtomography and computational simulation. *Soil Tillage Res.* **209**, 104941 (2021)
- L.F. Pires, R.C.J. Arthur, O.O.S. Bacchi, K. Reichardt, Representative Gamma-ray Computed Tomography Calibration for Applications in Soil Physics. *Brazilian J. Phys.* **41**, 21 (2011)
- H. Rogasik, I. Onasch, J. Brunotte, D. Jegou, O. Wendroth, Assessment of soil structure using X-ray computed tomography. *Geol. Soc. London, Spec. Publ.* **215**, 151 (2003)
- M. Torikoshi, Y. Ohno, M. Natsuhori, N. Ito, K. Uesugi, N. Yagi, T. Tsunoo, M. De, M. Endo, Dualenergy X-ray CT with a vertically expanded irradiation field. *Nucl. Instruments Methods Phys. Res. Sect. A Accel. Spectrometers, Detect. Assoc. Equip.* **580**, 996 (2007).
- W. Chaiphaksa, P. Limkitjaroenporn, H.J. Kim, J. Kaewkhao, The mass attenuation coefficients, effective atomic numbers and effective electron densities for GAGG:Ce and CaMoO₄ scintillators. *Prog. Nucl. Energy* **92**, 48 (2016)
- A.C.G. Fonseca, L.F. Costa, C.C. Dantas, R.J. Heck, S.B. Melo, A.C.D. Antonino, E.S. Barbosa, Precise determination of soil structure parameters in a X-ray and γ -ray CT combination methodology. *Prog. Nucl. Energy* **114**, 138 (2019)
- I. Kaplan, *Nuclear Physics*, 2nd edn. (Addison-Wesley Publishing Company, Massachusetts, 1977)
- A. H. Taqi, Q. A. M. Al Nuaimy, G. A. Karem, Study of the properties of soil in Kirkuk, IRAQ. *J. Radiat. Res. Appl. Sci.* **9**, 259 (2016)
- C.F. Matta, R.J. Gillespie, Understanding and Interpreting Molecular Electron Density Distributions. *J. Chem. Educ.* **79**, 1141 (2002)
- S. R. Manohara, S. M. Hanagodimath, K. S. Thind, and L. Gerward, On the effective atomic number and electron density: A comprehensive set of formulas for all types of materials and energies above 1keV. *Nucl. Instruments Methods Phys. Res. Sect. B Beam Interact. with Mater. Atoms* **266**, 3906 (2008).
- N. Kämpf, J. J. Marques, N. Curi, in *Pedol. Fundam.*, edited by J. C. Ker, N. Curi, C. E. G. R. Schaefer, and P. V. Torrado, 1st ed. (Sociedade Brasileira de Ciência do Solo, Viçosa) p. 343 (2012)
- M.A. Camargo, K.S. Kodum, L.F. Pires, How Does the Soil Chemical Composition Affect the Mass Attenuation Coefficient? A Study Using Computer Simulation to Understand the Radiation-Soil Interaction Processes. *Brazilian J. Phys.* **51**, 1775 (2021)
- P. Buringh, *Introduction to the Study of Soils in Tropical and Subtropical Regions*, 2nd edn. (Centre for Agricultural Publishing and Documentation, Wageningen, 1970)
- M. R. Ribeiro, L. Barros de Oliveira, J. C. de A. Filho, in *Pedol. Fundam.*, edited by J. C. Ker, N. Curi, C. E. G. R. Schaefer, and P. V. Torrado, 1st ed. (Sociedade Brasileira de Ciência do Solo, Viçosa, p. 343 (2012)
- M.E. Medhat, Application of gamma-ray transmission method for study the properties of cultivated soil. *Ann. Nucl. Energy* **40**, 53 (2012)
- G.C. Topp, Soil water content from gamma ray attenuation: A comparison of ionization chamber and scintillation detectors. *Can. J. Soil Sci.* **50**, 439 (1970)
- J.C.M. Oliveira, K. Reichardt, C.M.P. Vaz, D. Swartzendruber, Improved Soil Particle-Size Analysis by Gamma-Ray Attenuation. *Soil Sci. Soc. Am. J.* **61**, 23 (1997)
- M. J. Berger, J. H. Hubbell, S. M. Seltzer, XCOM: Photon cross sections database. *J. Chang, J. S. Coursey, R. Sukumar, D. S. Zucker, K. Olsen*, Novemb. 2010 (2021).
- O. Ozyurt, N. Altinsoy, Şİ Karaaslan, A. Bora, B. Buyuk, İ Erk, Calculation of gamma ray attenuation coefficients of some granite samples using a Monte Carlo simulation code. *Radiat. Phys. Chem.* **144**, 271 (2018)
- M. Elsafi, M.F. Alrashedi, M.I. Sayyed, I.F. Al-Hamarneh, M.A. El-Nahal, M. El-Khatib, M.U. Khandaker, H. Osman, A. El Askary, The Potentials of Egyptian and Indian Granites for Protection of Ionizing Radiation. *Materials (Basel)*. **14**, 3928 (2021)
- L.F. Pires, M.E. Medhat, Different methods of mass attenuation coefficient evaluation: Influences in the measurement of some soil physical properties. *Appl. Radiat. Isot.* **111**, 66 (2016)
- M.E. Medhat, L.F. Pires, R.C.J. Arthur, Analysis of photon interaction parameters as function of soil composition. *J. Radioanal. Nucl. Chem.* **300**, 1105 (2014)
- P. C. Teixeira, G. K. Donagemma, A. Fontana, W. G. Teixeira, editors, *Manual de Métodos de Análise de Solo*, 3rd ed. (EMBRAPA, Brasília, 2017)
- T.R. Ferreira, L.F. Pires, A.M. Brinatti, A.C. Auler, Surface liming effects on soil radiation attenuation properties. *J. Soils Sediments* **18**, 1641 (2018)
- L.F. Pires, Soil analysis using nuclear techniques: A literature review of the gamma ray attenuation method. *Soil Tillage Res.* **184**, 216 (2018)
- F. H. Attix, *Introduction to radiological physics and radiation dosimetry* (Wiley, 1986)
- G. Nelson D. Reilly, in *Passiv. Nondestruct. Assay Nucl. Mater.*, edited by D. Reilly, N. Ensslh, H. Smith Jr, and S. Kreiner, 1st ed. (U.S. Government Printing Office, Washington), p. 723 (1991)

34. M.E. Medhat, Study of the mass attenuation coefficients and effective atomic numbers in some gemstones. *J. Radioanal. Nucl. Chem.* **293**, 555 (2012)
35. L. F. Pires, F. A. M. Cássaro, V. Correchel, Use of nuclear techniques in soil science: A literature review of the Brazilian contribution. *Rev. Bras. Ciência Do Solo* **45**, (2021)
36. E.S.B. Ferraz, R.S. Mansell, *Determining water content and bulk density of soil by gamma ray attenuation methods*, 1st edn. (Institute of Food and Agricultural Sciences, University of Florida, Gainesville Fla, Agricultural Experiment Stations, 1979)
37. R. Cavararo, *Manual Técnico de Pedologia*, 2nd edn. (Instituto Brasileiro de Geografia e Estatística - IBGE, Rio de Janeiro, 2007)
38. Ø. Hammer, D.A.T. Harper, P.D. Ryan, PAST: Paleontological Statistics Software Package for Education and Data Analysis. *Palaeontol. Electron.* **4**, 9 (2001)
39. L.F. Pires, W.C. Leite, A.M. Brinatti, S.C. Saab, Radiation attenuation properties based on the quantification of soil components using the Rietveld Method. *Results Phys.* **12**, 2009 (2019)
40. L. F. Pires, L. V. Prandel, S. da C. Saab, A. M. Brinatti, A novel approach based on X-ray fluorescence and photon attenuation to the analysis of soils for forensic investigation. *Rev. Bras. Ciência Do Solo* **46**, (2022)
41. G. S. Mudahar, S. Modi, and S. Makhan, Total and partial mass attenuation coefficients of soil as a function of chemical composition. *Int. J. Radiat. Appl. Instrumentation. Part A. Appl. Radiat. Isot.* **42**, 13 (1991)
42. D.K. Gaikwad, P.P. Pawar, T.P. Selvam, Mass attenuation coefficients and effective atomic numbers of biological compounds for gamma ray interactions. *Radiat. Phys. Chem.* **138**, 75 (2017)

Publisher's Note Springer Nature remains neutral with regard to jurisdictional claims in published maps and institutional affiliations.